IJST, Transactions of Civil Engineering, Vol. 38, No. C2, pp 395-407
Printed in The Islamic Republic of Iran, 2014

PROPOSED EQUATIONS FOR ESTIMATING THE FLEXURAL CHARACTERISTICS OF REINFORCED HPFRCC BEAMS*

A. HEMMATI[1**], A. KHEYRODDIN AND[2] M. K. SHARBATDAR[3]

[1]Dept. of Civil Engineering, Semnan Branch, Islamic Azad University, Semnan, I. R. of Iran
Email: ahemmati2000@yahoo.com
[2, 3]Civil Engineering Faculty, Semnan University, Semnan, I. R. of Iran

Abstract– HPFRCC materials are a class of cement composites with fine aggregates that exhibit strain hardening behavior under tensile loading. This strain hardening response occurs after the first cracking of the material. In this paper, experimental and theoretical studies were conducted to assess the influence of using HPFRCC material instead of normal concrete in RC beams. The theoretical results for simply supported beams with different values of compressive strengths are presented and compared with the available experimental data. Results indicate that using HPFRCC material instead of normal concrete in RC beams concludes to more ultimate load, deflection and ductility compared to normal reinforced concrete beams. Moreover, new theoretical equations are proposed for estimating the flexural characteristics of reinforced composite and reinforced HPFRCC beams. Results show that the flexural capacity of reinforced HPFRCC beams is about 6.4% higher than that of RC beams. Moreover, flexural capacity of experimental reinforced HPFRCC beams is about 11.2% higher than that of theoretical values.

Keywords– Concrete, HPFRCC, flexural capacity, ultimate deflection, ultimate load

1. INTRODUCTION

High Performance Fiber Reinforced Cementitious Composite (HPFRCC) materials exhibit strain hardening behavior under uni-axial tensile loading. These materials are characterized by pseudo-ductile tensile strain hardening behavior and multiple cracking prior to failure [1]. High tensile ductility and strain hardening behavior are the most important characteristics of HPFRCC compared to normal concrete [2]. In recent years, a new class of HPFRCC has emerged as ECC. Engineered Cementitious Composites, developed at the University of Michigan had a typical moderate tensile strength of 4-6 MPa and ductility of 3-5% [3]. A number of researchers have developed ECC material based on PVA fibers. But using other types of fibers such as PP (Polypropylene) was successful and consequently, decision making on selection and use of the type of fiber, depends on natural characteristics of fibers such as diameter ranges, surface characteristics and mechanical behavior. It also depends on the matrix cracking properties, fiber-matrix interfacial bonding properties, the desired properties of the ECC composites, the durability needed, the desired sustainability of the system and the economic constraints of the application [4, 5].

The main part of the experimental tests which were conducted on reinforced HPFRCC beams focused on durability and steel corrosion of these members and it is necessary to evaluate the structural influence of using HPFRCC in RC beams. Some theoretical equations were proposed based on micro scale plasticity based models for simulating the behavior of reinforced HPFRCC flexural members too [6-14]. These plasticity based models are very complicated and there are no simple equations for estimating the flexural characteristics of reinforced HPFRCC beams. Consequently, it is necessary to propose some new and

*Received by the editors March 25, 2013; Accepted November 23, 2013.
**Corresponding author

simple equations for calculating the macro scale flexural characteristics of reinforced HPFRCC members. In this paper, an experimental work was conducted and then new theoretical equations based on the stress-strain curves of HPFRCC material were proposed to consider the influence of using HPFRCC material instead of normal concrete in RC beams.

2. EXPERIMENTAL PROGRAM

An experimental investigation was conducted to evaluate the behavior of reinforced concrete (RC), reinforced composite beams with different HPFRCC thicknesses (RCH) and reinforced HPFRCC (RH) beams under monotonic two-point loading. The test specimens which were chosen for this experimental study were five large scale beams with two hinge supports which were tested by the authors. The beam clear span was 2100 mm, total length was 2300 mm with constant cross section of 300 mm deep by 200 mm wide. Details of reinforcement layout and loading of these beams are shown in Fig. 1.

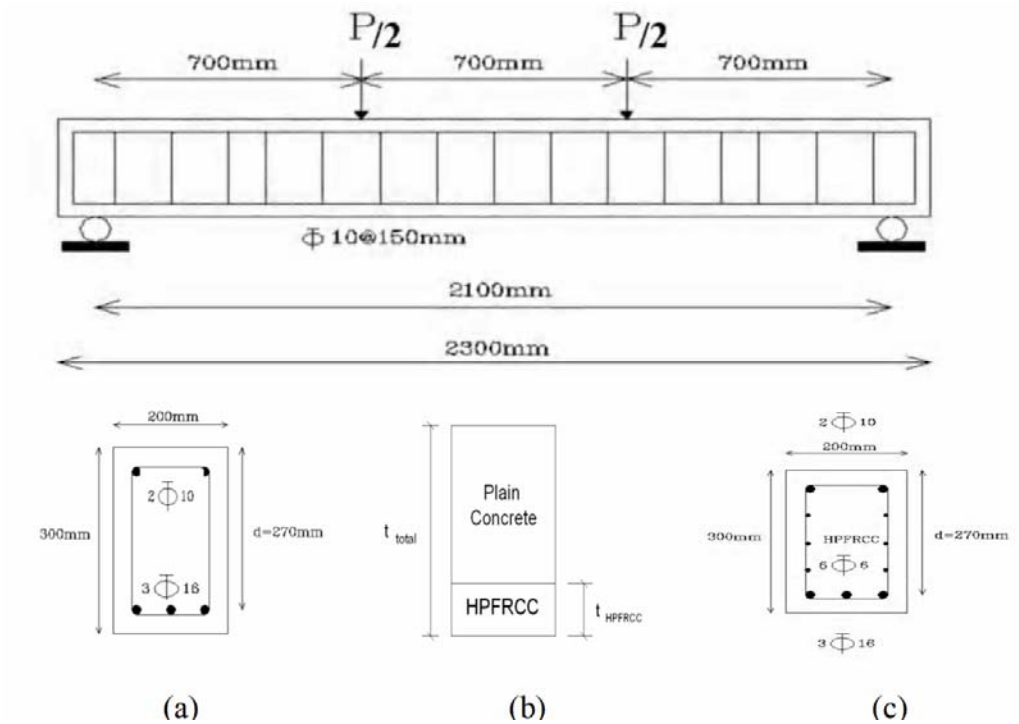

Fig. 1. Details of (a) RC, (b) RCH and (c) RH experimental specimen

As shown in this figure, reinforcement details of RC and RCH specimens were the same but some extra steel reinforcements were provided in RH specimen for assessing the strain distribution along the height of this section. Mix proportions of the concrete and HPFRCC materials are presented in Table 1. The mixture ratios were based on the weight of cement. Coarse aggregate was not used in HPFRCC material, but Polypropylene (PP) fibers with a length of 12 mm and diameter of 18 μm were used for achieving the HPFRCC. Coarse aggregate gradations taking 4.75 to 12.5 mm particles and fine aggregate gradations taking particles less than 4.75 mm were used too. During the mixing, care was taken to prevent clumping of the fibers. The dry components of the mortar mix were first combined with approximately 25% of the total water required and then the fibers along with the remaining 75% of the water were intermittently added as the mixing process progressed. The fibers were added slowly, while mixing continued in order to distribute the fibers thoroughly throughout the mix. To determine the compressive strengths of the concrete and HPFRCC material, compression test on 100 x 100 mm cubes specimens was

conducted as shown in Fig. 2a and compressive failure of these specimens is presented in Fig. 2b. As shown in this figure, due to the presence of PP fibers, the HPFRCC maintains its integrity under loading and consequently shows a ductile behavior. Material properties are summarized in Table 2.

Table 1. Mix proportion of concrete and HPFRCC (Based on the weight of cement)

Material	Cement	Coarse Aggregate	Fine Aggregate	Water	Fiber
Concrete	1	1.72	1.72	0.45	-
HPFRCC	1	-	1	0.54	1% (Volume Fraction)

Table 2. Concrete, HPFRCC and steel properties used in the experimental specimens

Material properties	Concrete	HPFRCC
$f_c'\ (MPa)$	35.7	24
$f_y\ (MPa)$	400	400

Test set up of RC, RCH and RH beams is presented in Fig. 3.

Fig. 2. Compression test of concrete and HPFRCC specimens

Fig. 3. Test Set-up

The vertical load was applied on RC beam with $\frac{t_{HPFRCC}}{t}$=0 and the first cracking observed at the load of 46 kN and mid-span deflection of 1.29 mm respectively at the mid-span of the beam. Then the yielding of steel bars occurred at the load of 161 kN and deflection of 5.97 mm. Further loading caused the cracking to spread at the bottom face of the beam and finally the beam carried the load of 239.83 kN and deflection of 30.25 mm. Condition of the RC beam at the ultimate load and displacement is shown in Fig. 4. As shown in this figure, the failure was in flexural mode, i.e. at first step tensile reinforcements started to yield and then compressive crushing of concrete occurred. The failure was accompanied by large tensile cracks in lower parts of the section at mid-span of the beam. The amount of damage in compressive concrete was severe and ultimate deflection was small.

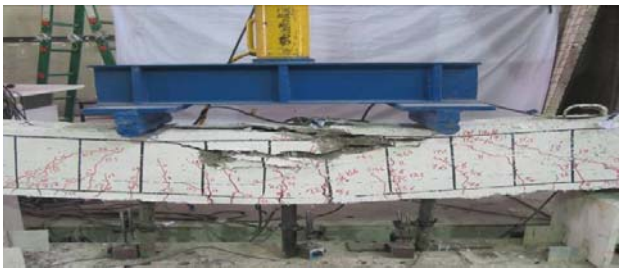

Fig. 4. General view of RC beam at the end of loading

Then, the vertical load was applied on RCH-0.2, RCH-0.4 and RCH-0.6 specimens with $\frac{t_{HPFRCC}}{t} =$ 0.2, 0.4 and 0.6 respectively according to Fig. 2b. During the loading process of RCH-0.2, it was observed that the crack width in lower HPFRCC part was less than that of upper concrete part as shown in Fig. 5.

Fig. 5. Crack width in concrete and HPFRCC in RCH-0.2

In the case of RH specimen with $\frac{t_{HPFRCC}}{t}=1$, the first cracking was observed at the load of 45 kN and mid-span deflection of 1.46 mm respectively at the mid-span of the beam and then the yielding of steel bars occurred at the load of 160 kN and deflection of 6.22 mm. Further loading caused the cracking to spread at the bottom face of the beam and finally the beam carried the load of 263.17 kN and deflection of 59.95 mm. Condition of the RH beam at the ultimate load and displacement is shown in Fig. 6.

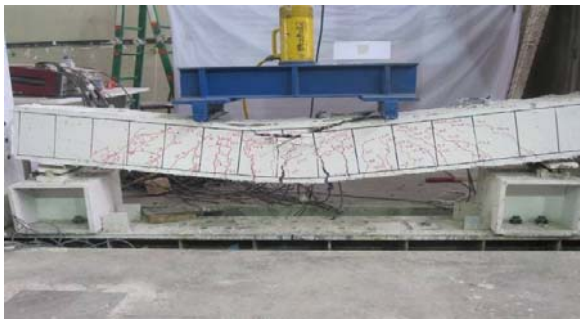

Fig. 6. General view of RH beam at the end of loading

Load-deflection curves of these five test specimens are presented in Fig. 7. Summary of these experimental results are presented in Table 3. Where, $\mu = \frac{\Delta_u}{\Delta_y}$.

Table 3. Summary of experimental results

Specimen	P_y (kN)	P_u (kN)	Δ_y (mm)	Δ_u (mm)	μ	$\frac{\mu}{\mu_{RC}}$
RC	161	239.83	5.97	30.25	5.07	1
RCH-0.2	169	264.33	6.5	36.61	5.63	1.11
RCH-0.4	167	275.5	6.7	41.15	6.14	1.21
RCH-0.6	175	255.17	6.54	45.86	7.01	1.38
RH	160	263.17	6.22	59.95	9.64	1.9

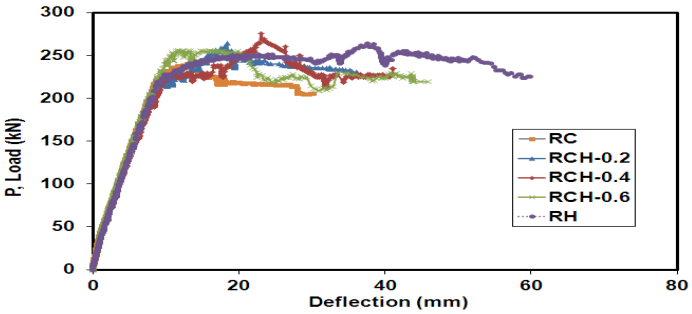

Fig. 7. Load-deflection curves of experimental specimens

As shown in this table, while the compressive strength of normal concrete is 35.7 MPa and about 1.5 times more than that of HPFRCC material, the ultimate load of RH beam is about 9.7 % higher than its corresponding value in RC specimen. This may be due to the existence of reinforcing fibers and HPFRCC material behaves as a ductile paste and maintains its integrity under severe loading (bridging mechanism and pull out of fibers) and subsequently steel reinforcements suffer more strains and get closer to the value of their plastic strain. This phenomenon results in higher ultimate load in the case of RH specimen compared to the RC one. This mechanism has the most important role on behavior of RH beam and this improving effect is more important than the magnitude of compressive strength of concrete. Strain distribution along the height of RH beam is presented in Fig. 8. It must be noted that because of existence of limited strain gauges installed on this specimen, these experimental values are approximate and more analytical works must be conducted for further exact responses which will be presented in future papers.

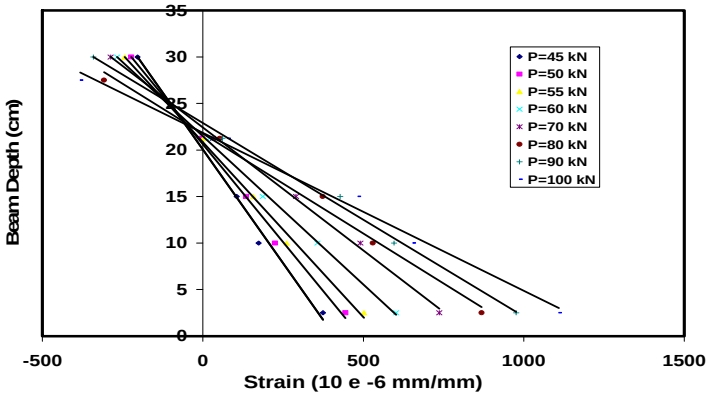

(a) From 45 to 100 kN

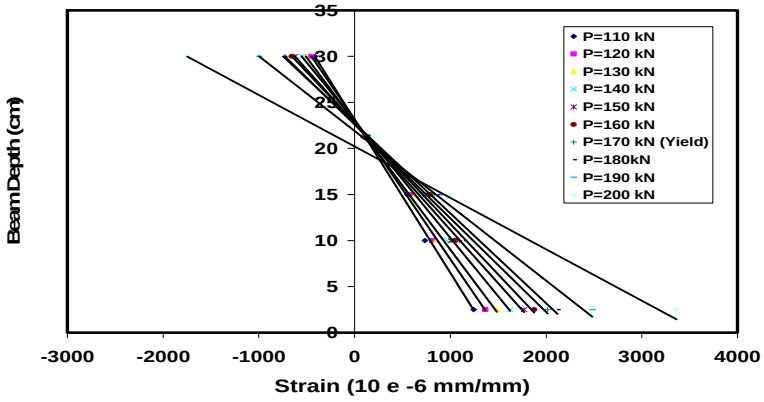

(b) From 110 to 200 kN

Fig. 8. Strain distribution along the height of RH specimen

As the compressive strength of concrete and HPFRCC material and reinforcement details of RC and RH specimens were different, another experimental work was conducted to evaluate the behavior of RC and RH beams with the same compressive strength (24 MPa) and reinforcement details under monotonic two-point loading. Details of reinforcement layout and loading of the beams are shown in Fig. 9. Load-deflection curves of these two test specimens are presented in Fig. 10. Summary of these experimental results are presented in Table 4.

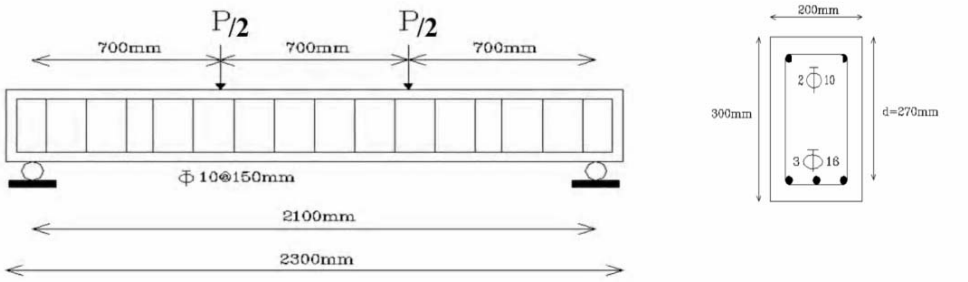

Fig. 9. Details of two specimens with the same compressive strength reinforcement details

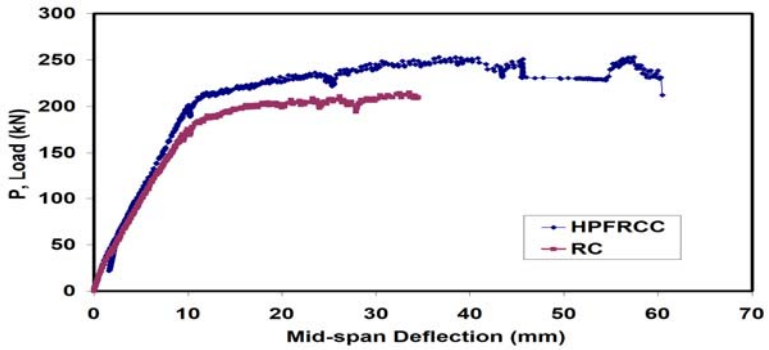

Fig. 10. Load-deflection curves of experimental specimens with the same compressive strength reinforcement details

Table 4. Experimental results for beams with the same compressive strength and reinforcement details

Specimen	Δ_y (mm)	P_u (kN)	Δ_u (mm)	μ	$\frac{\mu}{\mu_{RC}}$
RC	6.57	238.08	34.47	5.25	1
RH	6.66	253.44	60.45	9.08	1.73

As shown in this table, compressive strength of HPFRCC and concrete has no important influence on experimental results.

3. PROPERTIES OF HPFRCC

Some stress-strain relations were proposed to model the behavior of HPFRCC material in compression and tension [15-20]. In recent years, Hung and El-Tawil proposed two three-part curves to model HPFRCC material in compression and tension as shown in Fig. 11. In compression (Fig. 11a), the compressive stress starts from zero and progressively increases until reaching the peak compressive strength by a parabolic function. The first stage is then followed by a linear softening portion until the residual strength is reached. In the third part, the stress is assumed to remain constant at the level of plateau stress. The uniaxial stress-strain relationship of HPFRCC materials in tension is defined as shown in Fig. 11b. The first segment of the curve is the linear elastic portion, followed by strain hardening

behavior until crack localization occurs. After crack localization, the tensile behavior starts to linearly soften until it is no longer able to support tensile stress. These stages are discussed by Eq. (1) [21].

$$\sigma_c = \begin{cases} \sigma_{cp} \cdot \left[2\left(\dfrac{\varepsilon}{\varepsilon_{cp}}\right) - \left(\dfrac{\varepsilon}{\varepsilon_{cp}}\right)^2 \right] & if \quad 0 \le \varepsilon < \varepsilon_{cp} \\ \sigma_{cp} \cdot \left(1 - \dfrac{\varepsilon - \varepsilon_{cp}}{\varepsilon_{cu} - \varepsilon_{cp}}\right) & if \quad \varepsilon_{cp} \le \varepsilon < \varepsilon_{cu} \\ k_0 \cdot \sigma_{cp} & if \quad \varepsilon \ge \varepsilon_{cu} \end{cases} \quad and \quad \sigma_t = \begin{cases} \dfrac{\varepsilon}{\varepsilon_{tc}} \cdot \sigma_{tc} & if \quad 0 \le \varepsilon < \varepsilon_{tc} \\ \sigma_{tc} + (\sigma_{tp} - \sigma_{tc}) \cdot \left(\dfrac{\varepsilon - \varepsilon_{tc}}{\varepsilon_{tp} - \varepsilon_{tc}}\right) & if \quad \varepsilon_{tc} \le \varepsilon < \varepsilon_{tp} \\ \sigma_{tp} \cdot \left(\dfrac{\varepsilon - \varepsilon_{tp}}{\varepsilon_{tu} - \varepsilon_{tp}}\right) & if \quad \varepsilon_{tp} \le \varepsilon \le \varepsilon_{tu} \\ 0 & if \quad \varepsilon_{tu} \le \varepsilon \end{cases} \tag{1}$$

Where, E = young modulus, σ_{cp} = maximum compressive stress, ε_{cp} = strain corresponding to maximum compressive stress, ε_{cu} = ultimate compressive strain, ε_{t0} = first cracking strain, σ_{tp} = peak tensile stress, ε_{tp} = strain corresponding to maximum tensile stress and ε_{tu} = ultimate tensile strain.

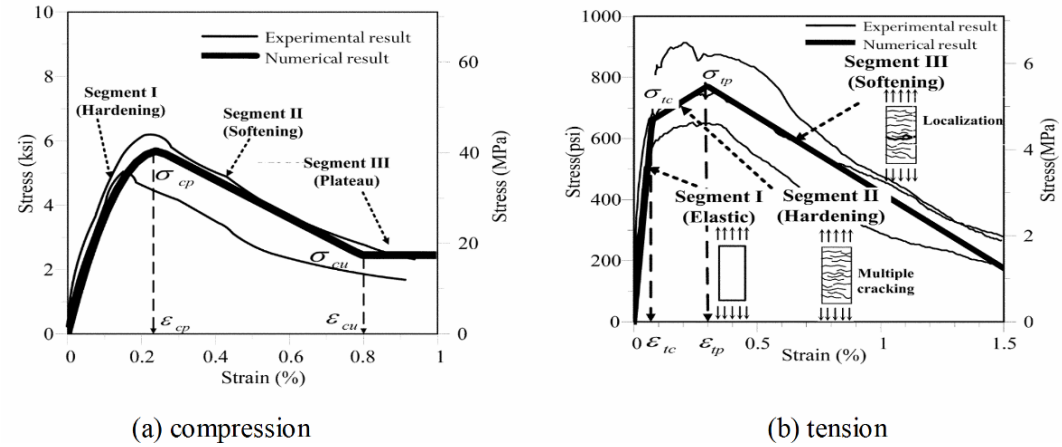

(a) compression (b) tension

Fig. 11. Stress-strain curves of HPFRCC [17]

4. NEW PROPOSED EQUATIONS FOR HPFRCC

a) Equivalent whitney compression stress block of HPFRCC

An idealized tension and compression stress-strain curves of HPFRCC material is illustrated in Fig. 12. Idealization in tension part was modeled by an elastic-perfect plastic curve. Idealization in compression part may follow that of normal concrete using the Whitney stress block. Compressive behavior of HPFRCC may not be significantly different from that of normal concrete. Compressive strain capacity of HPFRCC is higher and its post-peak softening branch is gentler than those of normal concrete [15-18]. These features may necessitate the recalibration of the values of α and β_1 for calculating the flexural characteristics of HPFRCC members [22].

Two important criteria are employed for calculating the values of α and β_1 in HPFRCC beams as follows:

- Area under the real HPFRCC compressive stress-strain curve (solid line in Fig. 13) must be equal to that of equivalent rectangular stress block (dashed line in Fig. 13).
- Area centers of the HPFRCC real compressive stress-strain curve and equivalent rectangular stress block must be the same.

The ultimate strain of HPFRCC is assumed to occur when stress degradation of this material is equal to 15 %.

$$\begin{aligned}
&\overline{X}_{total} = \frac{\bar{x}_1 A_1 + \bar{x}_2 A_2}{A_{total}} \\
&A_{total} = A_1 + A_2 \\
&A_{total} = \int_0^{\varepsilon_{cp}} f_c' \left[2\left(\frac{\varepsilon}{\varepsilon_{cp}}\right) - \left(\frac{\varepsilon}{\varepsilon_{cp}}\right)^2 \right] .d\varepsilon + \int_{\varepsilon_{cp}}^{\varepsilon_{cu}} f_c' \left(1 - \frac{\varepsilon - \varepsilon_{cp}}{\varepsilon_{cu} - \varepsilon_{cp}} \right) .d\varepsilon \\
&A_{equivalent} = \alpha \cdot f_c' \cdot 2 \cdot \left(\varepsilon_{cu} - \overline{X}_{total} \right) \\
&A_{total} = A_{equivalent} \\
&\left(\varepsilon_{cu} - \overline{X}_{total} \right) \times 2 = \beta_1 \cdot \varepsilon_{cu}
\end{aligned} \tag{2}$$

Where, $\overline{X}_{total}$ = area center of HPFRCC real compressive stress-strain curve, $\bar{x}_1$, $\bar{x}_2$ = area centers of first parabolic and second linear parts of real compressive stress-strain curve of HPFRCC and A_1, A_2 = area of first and second parts of the real compressive stress-strain curve of HPFRCC. The following equations are obtained using Eqs. (1) and (2.)

$$\alpha = \frac{\left[\frac{2}{3}\varepsilon_{cp} + 0.925 \cdot \left(\varepsilon_{cu} - \varepsilon_{cp} \right) \right]^2}{2 \cdot \left[\frac{2}{3}\varepsilon_{cu} \cdot \varepsilon_{cp} + 0.925\varepsilon_{cu} \cdot \left(\varepsilon_{cu} - \varepsilon_{cp} \right) - \frac{5}{12}{\varepsilon_{cp}}^2 - \left(\varepsilon_{cu} - \varepsilon_{cp} \right) \cdot \left[0.925\varepsilon_{cp} + \frac{2.7}{6} \cdot \left(\varepsilon_{cu} - \varepsilon_{cp} \right) \right] \right]}$$

$$\beta_1 = \frac{2 \cdot \left[\frac{2}{3}\varepsilon_{cu} \cdot \varepsilon_{cp} + 0.925\varepsilon_{cu} \cdot \left(\varepsilon_{cu} - \varepsilon_{cp} \right) - \frac{5}{12}{\varepsilon_{cp}}^2 - \left(\varepsilon_{cu} - \varepsilon_{cp} \right) \cdot \left[0.925\varepsilon_{cp} + \frac{2.7}{6} * \left(\varepsilon_{cu} - \varepsilon_{cp} \right) \right] \right]}{\varepsilon_{cu} \cdot \left[\frac{2}{3}\varepsilon_{cp} + 0.925 \cdot \left(\varepsilon_{cu} - \varepsilon_{cp} \right) \right]} \tag{3}$$

It is observed that values of α and β_1 for HPFRCC sections are different from corresponding values in normal concrete and dependent on ε_{cu} and ε_{cp} of HPFRCC material as observed in Table 5. In a normal concrete section, $\alpha = 0.85$ and β_1 is calculated by Eq. (4) [23]. Where, $\alpha_{(NC)} = 0.85$ and $\beta_{1(NC)} = 0.85$ are related to normal concrete.

$$\beta_1 = \begin{cases} 0.85 \quad if \quad f_c' \le 280 \, {kg}/{cm^2} \\ 0.85 - 0.05\dfrac{f_c' - 280}{70} \quad if \quad 280 < f_c' < 560 \, {kg}/{cm^2} \\ 0.65 \quad if \quad f_c' \ge 560 \, {kg}/{cm^2} \end{cases} \tag{4}$$

Table 5. Comparison between analytical values of α and β_1 for RH beams

ε_{cp}	ε_{cu}	α	β_1	$\frac{\alpha}{\alpha_{(NC)}}$	$\frac{\beta_1}{\beta_{1(NC)}}$
0.002	0.0029	0.9074	0.823	1.067	0.968
0.004	0.0046	0.899	0.779	1.057	0.916

As shown in this table, these theoretical values are close to that of RC beams. Because the compressive behavior of concrete and HPFRCC are approximately the same.

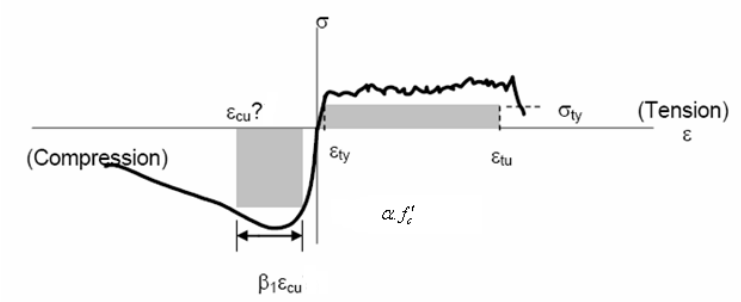

Fig. 12. Idealized stress-strain curve of HPFRCC [18]

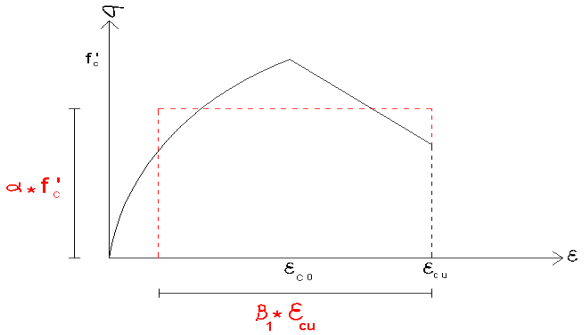

Fig. 13. Real HPFRCC compressive stress-strain curve and equivalent rectangular block

b) Flexural capacity of RH beams

Strain and stress distributions along the height of a flexural rectangular HPFRCC section are observed in Fig. 14. It is assumed that the strain distribution along the height of the section is linear according to Fig. 8. As shown in this figure, the depth of the equivalent compressive stress block ($a = \beta_1 c$) and flexural capacity of a HPFRCC section (M_r) can be calculated by Eq. (5).

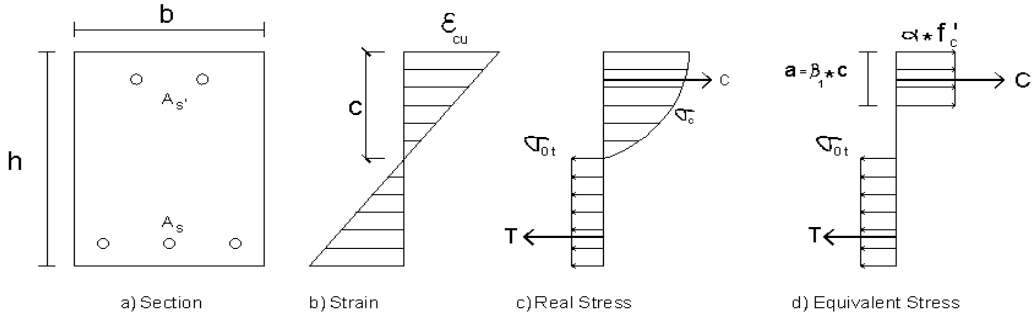

Fig. 14. Strain and stress distributions in a flexural rectangular HPFRCC section

$$\sum F_x = 0 \Rightarrow \alpha.f'_c.a.b + A_s' \cdot f_y - A_s.f_y - \sigma_{0t}.b.(h-c) = 0$$

$$a = \frac{(A_s - A_s').f_y + \sigma_{0t}.b.h}{\alpha.f'_c.b + \sigma_{0t}.\dfrac{b}{\beta_1}} = \beta_1.c$$

$$M_r = \alpha.f'_c.a.b.\left(d - \frac{a}{2}\right) + A_s' \cdot f_y \cdot (d - d') - \sigma_{0t}.b.(h-c).\left[\left(\frac{h-c}{2}\right) - (h-d)\right] \quad (5)$$

Where, f'_c = compressive strength of HPFRCC, b = width of the member, f_y = tensile strength of reinforcements, A_s = area of tensile reinforcements, A'_s = area of compressive reinforcements, σ_{0t} = tensile strength of HPFRCC, h = height of the member and d = effective height of the member.

Flexural capacity of RC and RH beams are calculated using Eq. (5) ($M_r(Theo.)$) and compared with available experimental values ($M_r(Exp.)$) in Table 6.

Table 6. Experimental and theoretical results for RC and RH beams

Beam	σ_{0t} (MPa)	f_c' (MPa)	α	β_1	a (mm)	$M_r(Theo.)$ (kN.m)	$M_r(Exp.)$ (kN.m)	$\frac{M_r(Theo.)}{M_r(Exp.)}$
RC	-	24	0.85	0.85	43.73	59.34	83.33	0.71
RC	-	35.7	0.85	0.795	29.39	60.62	83.94	0.72
RH	3.5	24	0.9074	0.823	74.61	79.74	88.7	0.9

As shown in this table, because of strain hardening behavior of HPFRCC material the equivalent neutral axis depth (a) and flexural capacity of RH beam are higher than that of RC beams. Theoretical values of flexural capacity of RC beams are about 28.5 % less than that of experimental values. This difference may be due to post yielding increase in tensile reinforcement forces of RC beams and tensile part of concrete which were ignored in theoretical formulation of these beams. The flexural capacity of RH beam is about 10 % less than that of experimental value. This difference may be due to post yielding increase in tensile reinforcement forces of RH beams which were ignored in this formulation too. As shown in this Table, theoretical and experimental values of M_r in reinforced HPFRCC members are close to each other and therefore this equation can be used for estimating the flexural capacity of RH beams.

c) Maximum reinforcement ratio of RC beams with tensile HPFRCC

Maximum reinforcement ratio of these beams can be calculated as shown in Eq. (6).

$$0.85.f_c'.a_b.b + A_s'.f_y - A_s.f_y - \sigma_{0t}.b.t_{HPFRCC} = 0$$
$$a_b = \beta_1 c_b$$
$$\varepsilon_{cu} = 0.003$$
$$c_b = \frac{630}{630 + f_y}.d$$
$$0.85.f_c' \cdot \beta_1 \cdot \frac{630}{630 + f_y}.d \cdot b + A_s'.f_y = A_s.f_y + \sigma_{0t}.b.t_{HPFRCC}$$

then,

$$\rho - \rho' \le \rho_b - \frac{\sigma_{0t}}{f_y}.\frac{t_{HPFRCC}}{d}$$
$$\rho - \rho' \le \overline{\rho} \qquad (6)$$

where, ρ = tensile reinforcement ratio, ρ' = compressive reinforcement ratio, ρ_b = maximum reinforcement ratio in RC beams ($\rho_b = \alpha.f_c'.\beta_1.\frac{630}{630 + f_y}.\frac{1}{f_y}$) and $\overline{\rho}$ = maximum reinforcement ratio in beams with tensile HPFRCC part ($\overline{\rho} = \rho_b - \frac{\sigma_{0t}}{f_y}.\frac{t_{HPFRCC}}{d}$).

As could be seen in Eq. (6), the amount of maximum reinforcement ratio in partially tensile HPFRCC beams is less than its corresponding value in normal reinforced concrete beams. Tensile part of HPFRCC acts as an extra reinforcement and results in less maximum reinforcement ratio compared to normal concrete. This equation was derived based on theoretical concepts and more experimental tests must be conducted to achieve more exact responses and formulations.

d) Minimum reinforcement ratio in RH beams

When the tension reinforcement ratio becomes extremely small in a RC member, the yielding moment (M_r) becomes smaller than the cracking moment (M_{cr}) and steel bars may yield immediately after cracking, also the member shows brittle failure mode with only one crack like un-reinforced concrete [16]. This requires the tensile reinforcement ratio (ρ) of a rectangular beam to be larger than $\frac{1.4}{f_y}$ in ACI code [19]. Minimum reinforcement ratio in a RH beam ($\rho_{\min}$) can be calculated by:

$$M_{cr} = M_r \qquad M_r = \alpha.f'_c.a.b.\left(d-\frac{a}{2}\right)-\sigma_{0t}.b.(h-c).\left[\left(\frac{h-c}{2}\right)-(h-d)\right]$$

$$M_{cr}=\frac{\sigma_{0t}\cdot I_g}{y_t}=\frac{1}{6}\sigma_{0t}.b.h^2 \qquad \frac{1}{6}\sigma_{0t}.b.h^2=\alpha.f'_c.a.b.\left(d-\frac{a}{2}\right)-\sigma_{0t}.b.(h-c).\left[\left(\frac{h-c}{2}\right)-(h-d)\right]$$

It is known that: $c=\frac{\varepsilon_{cu}}{\varepsilon_{cu}+\varepsilon_y}\times d$, $a=\beta_1\cdot c$ Then,

$$d-\frac{a}{2}=d-\frac{\beta_1.c}{2}=d-\frac{\beta_1\cdot\varepsilon_{cu}}{(\varepsilon_{cu}+\varepsilon_y)\times 2}\times d=\left(1-\frac{\beta_1\cdot\varepsilon_{cu}}{(\varepsilon_{cu}+\varepsilon_y)\times 2}\right)\cdot d=\gamma\cdot d$$

$$h-c=h-\frac{\varepsilon_{cu}}{(\varepsilon_{cu}+\varepsilon_y)}\times d=\left(1.1-\frac{\varepsilon_{cu}}{(\varepsilon_{cu}+\varepsilon_y)}\right)\cdot d=\phi\cdot d$$

$$\alpha\cdot f'_c\cdot a\cdot b=A_s\cdot f_y+\sigma_{0t}\cdot b\cdot(h-c)$$

$$h=1.1\times d$$

$$\frac{1}{6}\sigma_{0t}.b.h^2=A_s\cdot f_y\cdot\gamma\cdot d+\sigma_{0t}\cdot b\cdot\phi\cdot d\cdot\gamma\cdot d-\sigma_{0t}.b.\phi.d\cdot\left[\frac{\phi\cdot d}{2}-(h-d)\right]$$

$$\frac{1}{6}\sigma_{0t}.b\times 1.21\times d^2=\rho\cdot b\cdot d\cdot f_y\cdot\gamma\cdot d+\sigma_{0t}\cdot b\cdot\phi\cdot d\cdot\gamma\cdot d-\sigma_{0t}.b.\phi.d\cdot\left[\frac{\phi\cdot d}{2}\right]$$

$$h-d\approx 0$$

$$\rho_{\min}=\frac{[0.2-\phi\cdot\gamma+\frac{\phi^2}{2}]\cdot\sigma_{0t}}{f_y\cdot\gamma} \tag{7}$$

As could be seen in Eq. (7), the amount of $\rho_{\min}$ depends on values of β_1, ε_{cu}, ε_y and σ_{0t} shown in Table 7. As shown in this table, the amount of minimum tensile reinforcement for RH beams is related to tensile strength of HPFRCC and yielding stress of longitudinal reinforcements. In the case of a RH beam with σ_{0t} = 5 MPa, the amount of $\rho_{\min}$ is 0.24 times that of normal concrete. This equation was derived based on theoretical concepts and more experimental tests must be conducted to achieve more exact responses and formulations too.

Table 7. Theoretical values of $\rho_{\min}$ for RH beams

β_1	ε_{cu}	ε_y	$\rho_{\min}$ (HPFRCC)	σ_{0t} = 5 MPa	$\frac{\rho_{\min}}{\rho_{\min-ACI}=\frac{1.4}{f_y}}$
0.823	0.008	0.002	$\rho_{\min}=\frac{0.0652\cdot\sigma_{0t}}{f_y}$	$\rho_{\min}=\frac{0.326}{f_y}$	0.24

5. CONCLUSION

1) Compressive behavior of HPFRCC may not be significantly different from that of normal concrete; hence, the equivalent compressive stress block could be used for calculating the flexural capacity of

HPFRCC members. The proposed values for α and β_1 are close to normal concrete and the difference is about 8%.

2) Using HPFRCC in the bottom of the normal reinforced concrete beams results in increase of the ultimate load, ductility, compressive stress block depth (a) and flexural capacity of the member (M_r).

3) Flexural capacity of reinforced HPFRCC beams is about 6.4% higher than that of RC beams. Flexural capacity of experimental reinforced HPFRCC beams is about 11.2% higher than that of theoretical values too.

4) The amount of maximum reinforcement ratio in RCH beams is less than that of RC beams. Because tensile part of HPFRCC acts as an extra reinforcement which results in less reinforcement ratio compared to normal concrete.

5) The amount of minimum reinforcement ratio in RH beams is related to values of β_1, ε_{cu}, ε_y, tensile strength of HPFRCC and yielding stress of longitudinal reinforcements and is usually less than the corresponding values in RC beams. In the case of a RH beam with σ_{0t} = 5 MPa, the amount of $\rho_{\min}$ is 0.24 times that of normal concrete.

REFERENCES

1. Li, V. C. & Wu, H. C. (1992). Conditions for pseudo strain-hardening in fiber reinforced brittle matrix composites. *J. Applied Mechanics Review*, Vol. 45, No. 8, pp. 390-398.
2. Naaman, A. E. & Reinhardt, H. W. (1996). Characterization of high performance fiber reinforced cement composites. HPFRCC-2, pp. 1-24.
3. Fischer, G. & Li, V. C. (2000). Structural composites with ECC. ASCCS-6, pp. 1001-1008.
4. Lee, B. Y., Kim, J. K. & Kim, Y. Y. (2010). Prediction of ECC tensile stress-strain curves based on modified fiber bridging relations considering fiber distribution characteristics. *Computers and Concrete, An Int'l Journal*, Vol. 7, No. 5.
5. Sadrmomtazi, A. & Fasihi, A. (2010). Influence of polypropylene fibers on the performance of Nano-Sio2-Incorporated mortar. *Iranian Journal of Science and Technology, Transaction B: Engineering*, Vol. 34, No. B4, pp. 385-395.
6. Maalej, M. & Li, V. C. (1995). Introduction of strain hardening engineered cementitious composites in design of reinforced concrete flexural members for improved durability. *ACI Structural Journal*, Vol. 92, No. 2.
7. Maalej, M., Ahmed, S.F.U. & Paramasivam, P. (2002). Corrosion durability and structural response of functionally-graded concrete beams. *JCI International workshop on ductile fiber reinforced Cementitious composites(DFRCC)-Application and Evaluation*, Japan, pp. 161-170.
8. Li, V. C., Mihashi, H., Wu, H.C., Alwan, J. C., Brincker, R., Horii, H., Leung, C., Maalej, M. & Stang, H. (1996). Micromechanical models of mechanical response of HPFRCC", HPFRCC-2.
9. Kabele, P. (2000). Assessment of structural performance of engineered cementitious composites by computer simulation. Habilitation Thesis, Csech Technical University in Prague, pp. 46–50.
10. Szerszen, M. M. & Szwed, A. & Li, V. C. (2006). Flexural response of reinforced beam with high ductility concrete materials. *Brittle Matrix Composite*, Vol. 8.
11. Nielsen, L. D. (2008). Modeling of ECC materials using numerical formulations based on plasticity. PhD Dissertation, Technical University of Denmark.
12. Sirijaroonchai, K. (2009). A macro-scale plasticity model for high performance fiber reinforced cement composites. PhD Dissertation, Michigan University.
13. Hemmati, A., Kheyroddin, A. & Sharbatdar, M. K. (2013). Using HPFRCC for increasing the capacity of R.C. frame. *Sharif Civil Engineering Journal*, Vol. 29, No. 2.

14. Hemmati, A., Kheyroddin, A. & Sharbatdar, M. K. (2013). Plastic hinge rotation capacity of Reinforced HPFRCC beams'. *Journal of Structural Engineering (ASCE)*, DOI: 10.1061/(ASCE)ST.1943-541X.0000858, 2013.
15. Han, T. S., Feenstra, P. H. & Billington, S. L. (2003). Simulation of highly ductile fiber-reinforced cement-based composite components under cyclic loading. *ACI Structural Journal*, Vol. 100, No. 6, pp. 749-757.
16. Tokui, N., Sakai, Y., Sanada, Y., Yamauchi, N., Nakano, Y., Suwada, H. & Fukuyama, H. (2004). Simplified shaking table test methodology using extremely small scaled models. *13th World Conference on Earthquake Engineering*, Canada.
17. Qian, S. & Li, V. C. (2008). Simplified inverse method for determining the tensile properties of strain hardening cementitious composites. *Journal of Advanced Concrete Technology*, Vol. 6, No. 2, pp. 353-363.
18. JSCE, (2008). Recommendations for design and construction of high performance fiber reinforced cement composites.
19. Gencturk, B. & Elnashai A. S. (2009). Analytical modeling of engineered cementitious composite members. *Proceeding of ANCER Workshop*, University of Illinois.
20. Gencturk, B. & Elnashai, A. S. (2013). Numerical modeling and analysis of ECC structures. *Materials and Structures*, Vol. 46, No. 4, pp. 663-682.
21. Hung, C. C. & El-Tawil, S. (2010). Hybrid rotating/fixed-crack model for high performance fiber reinforced cementitious composites. *ACI Materials J*., pp. 568-576.
22. Li, V. C. & Rokugo, K. (2005). Task group D conclusions-HPFRCC design assumptions. *HPFRCC Workshop*, Hawaii.
23. ACI (2005). Building code requirements for structural concrete and commentary. ACI 318M-05.